

Article

Understanding Plugging Agent Emplacement Depth with Polymer Shear Thinning: Insights from Experiments and Numerical Modeling

Shanbin He ¹, Chunqi Xue ², Chang Du ², Yahui Mao ², Shengnan Li ², Jianhua Zhong ³, Liwen Guo ⁴ and Shuoliang Wang ^{4,*}

¹ Oilfield Development Division, Changqing Oilfield Company, Xi'an 710021, China; hsb_cq@petrochina.com.cn

² Petroleum Technology Research Institute, Changqing Oilfield Company, Xi'an 710021, China; xuechunqi0223@163.com (C.X.); changd_cq@petrochina.com.cn (C.D.); myhpetroleum@163.com (Y.M.); lishengnan_lsn@163.com (S.L.)

³ Qinhuangdao Campus, Northeastern University, Qinhuangdao 066004, China; zhongjhcq@163.com

⁴ School of Energy, China University of Geosciences, Beijing 100190, China; guoliwenlw@163.com

* Correspondence: wangshuoliang@cugb.edu.cn

Abstract: Polymer-plugging agents are widely employed in profile control and water-plugging measures, serving as a crucial component for efficient reservoir development. However, quantitatively monitoring the emplacement depth of polymer-plugging agents in low-permeability and high-permeability layers remains a challenging bottleneck. Presently, insufficient attention on shear thinning, a critical rheological property for water shut-off and profile control, has limited our understanding of polymer distribution laws. In this study, polymer shear-thinning experiments are firstly conducted to explore polymer variations with flow rate. The novelty of the research is that varying polymer viscosity is implemented instead of the fixed-fluid viscosity that is conventionally used. The fitted correlation is then integrated into the 2D and 3D heterogeneous numerical models for simulations, and a multivariate nonlinear regression analysis is performed based on the simulation results. The results show that lower polymer emplacement depth ratios corresponded to higher viscosity loss rates under the same flow rate. An increase in the initial permeability ratio corresponds to a decrease in the emplacement ratio, along with a reduction in the fraction of the plugging agent penetrating the low permeability formations. The model was applied to the Kunan Oilfield and demonstrated a polymer reduction of approximately 3000 tons compared to traditional methods. Despite the slightly complex nature of the multivariate nonlinear mathematical model, it presents clear advantages in controlling plugging agent distribution and estimating dosage, laying good theoretical ground for the effective and efficient recovery of subsurface resources.

Keywords: shear thinning; component model; numerical simulation; plugging agent; profile control



Citation: He, S.; Xue, C.; Du, C.; Mao, Y.; Li, S.; Zhong, J.; Guo, L.; Wang, S. Understanding Plugging Agent Emplacement Depth with Polymer Shear Thinning: Insights from Experiments and Numerical Modeling. *Processes* **2024**, *12*, 893. <https://doi.org/10.3390/pr12050893>

Academic Editors: Zhixue Sun and Xiaoguang Wang

Received: 16 March 2024

Revised: 17 April 2024

Accepted: 26 April 2024

Published: 28 April 2024



Copyright: © 2024 by the authors. Licensee MDPI, Basel, Switzerland. This article is an open access article distributed under the terms and conditions of the Creative Commons Attribution (CC BY) license (<https://creativecommons.org/licenses/by/4.0/>).

1. Introduction

Profile control and water shutoff represent widely employed techniques for stabilizing oil production and regulating water flux [1,2]. This method holds particular significance in oil fields characterized by predominant fluid flow through specific channels [3–5]. Throughout the process of profile control and water shutoff, variations in injection pressure and velocity exert influence on the distribution of plugging agents within reservoirs [6]. Polymer-plugging agents stand out as the most frequently utilized approach for profile control. However, challenges arise due to the non-Newtonian fluid characteristics and unique gelation kinetics of polymers, complicating the determination of distribution regularities, especially within heterogeneous reservoirs [7–9].

Scholars have investigated the distribution of plugging agents using seepage mechanics and numerical simulation [10,11]. Applying the principles of mass conservation and Darcy's law, Scott derived expressions for linear displacement and plane radial flow displacement, explicating the injection volume of the monomer gel-plugging agent [12]. Scott's work, however, exhibits a limitation in that it does not quantitatively assess the seepage behavior of polyacrylamide or xanthan sealants. To develop a more comprehensive model, Seright drew upon the studies by Deppe J C, particularly his work on injection rates, mobility ratio, area swept, and pattern effects [13–15]. This approach considered plugging agent viscosity, formation water viscosity, and formation porosity as constants, thereby elucidating the impact of the polymer injection resistance coefficient, chemical retention, dispersion, and diffusion on polymer agent emplacement. Nevertheless, the oversimplification of constant parameters by Seright resulted in noticeable errors in the calculation of the plugging agent emplacement ratio [16,17].

In summary, both Scott and Seright's methodologies are analytical, relying on assumptions that may introduce biases in practical applications. Notably, they fall short in estimating variations in polymer emplacement and describing changes in fluid viscosity within heterogeneous reservoirs. To address these challenges, significant contributions have been made by various scholars. For instance, Wang established a black oil model for the oil–water phase, enabling the calculation of the plugging agent emplacement rate [18]. The numerical model incorporates factors such as the residual resistance coefficient, adsorption capacity, and oil–water viscosity ratio. However, the specific influence of the shear-thinning characteristics of plugging agents on their distribution was not explicitly delineated [19]. In the context of deep profile control in heterogeneous reservoirs, the distinct flow velocities of plugging agents result in varying shear deformations [20]. This dynamic process leads to continuous changes in the viscosity of polymer agents. The time-varying viscosity, in turn, significantly impacts the distribution patterns of plugging agents in heterogeneous reservoirs, resulting in varied injection amounts of these agents [21].

This paper endeavors to elucidate the impact of shear-thinning characteristics on the distribution of plugging agents. Presently, various tools are employed for studying the shear-thinning properties of polymer-plugging agents, including corrugated mixers, high-speed mixers, sand-filled tubes, artificial cores, Wu Yin mixers, and sieve meshes. To introduce variable parameters for simulation, diverse methods generating shear-thinning effects were utilized to measure viscosity changes with the flow rate. Specifically, polymer solutions were subjected to high shearing rates in a corrugated mixer [22], Wu Yin agitator [23], high-speed stirrer [24], and conventional agitators. Alternatively, shear-thinning effects were examined by injecting polymer solutions through a sieve mesh [25] and artificial cores [26]. Recognizing that mixers or agitators may inadequately characterize shear effects in porous media, and the sieve mesh method is applicable primarily to homogeneous reservoirs, this study relies on artificial cores to explore the shear-thinning impact on polymer viscosity in heterogeneous reservoirs for more practical applications.

To summarize, the current characteristics and application of water-plugging agents in the oil field have the following deficiencies:

1. For the experiments on the shear-thinning properties of water-plugging agents, the commonly used methods (such as stirrers and sieve meshes) are obviously different from the shear effect on the flow of water-plugging agents in porous media reservoirs;
2. Previous studies have calculated the depth ratio of a water-plugging agent into the reservoir, but have not considered the effect of shear thinning on the depth ratio of a polymer-based plugging agent into the reservoir;
3. The previous research is not sufficient to investigate the different emplacement performance of water-plugging agents in high-permeability reservoirs and low-permeability reservoirs, and lacks a systematic analysis and summary of the influence of key factors such as the residual resistance coefficient, cumulative injection volume, permeability extreme difference and average injection rate.

Aiming to address the above research gaps, the following innovative work has been carried out in this study:

1. For the experiments on the shear thinning characteristics of the plugging agent, the artificial core can more realistically simulate the situation of non-homogeneous reservoirs, and the shear effect on the flow of the plugging agent in the artificial core is the closest to the flow of the plugging agent in the real reservoir; therefore, the artificial core method is chosen;
2. A variable viscosity–velocity rate formula for polymer-based plugging agents is proposed to make up for the lack of constant viscosity, which makes the calculation of the depth of the plugging agent into the reservoir more accurate;
3. In the numerical simulation, the control variable method is employed to examine the influences of four key parameters on the emplacement of polymer agents in different permeability layers. These parameters include the residual resistance coefficient, cumulative injection volume, average injection rate, and initial permeability ratio.

This study adopts an integrated approach encompassing the research stages of “in-door experiment—numerical simulation—optimization fitting.” The experimental phase involves conducting shear-thinning tests on four types of polymer-plugging agents within artificial cores, from which correlation curves for the emplacement ratio of polymer-plugging agents are derived. Subsequently, these correlation curves are incorporated into 2D and 3D numerical models to analyze the impact of shear thinning on the distribution of polymer agents. As a concluding step, a multivariate nonlinear regression model is developed, utilizing the aforementioned four parameters as variables, to predict the emplacement rate of polymer-plugging agents in both high- and low-permeability layers.

The novelty of the research is that varying polymer viscosity is implemented instead of the fixed-fluid viscosity that is conventionally used. The proposed model and established regression model are conducive to the understanding of the plugging agent distribution and dosage estimation, which lays a good theoretical foundation for effective and efficient reservoir exploitation, especially the secondary recovery of crude oil.

2. Experiment

2.1. Materials and Apparatus

The artificial cores utilized in this study were fabricated through the compression and sintering of quartz sands. These cores possess dimensions of 2.5 cm in diameter and 30 cm in length, featuring an average permeability of 0.8 Darcy and an average porosity of 26.05% (Figure 1a). The simulated brine used has a salinity of 508 mg/L and is employed to prepare the mother solution. The chemical agent employed is the salt-resistant polymer KYPAM, characterized by a relative molecular weight of 2.6×10^7 and a solid content of 90.86%. The mother solution, with a concentration of 5000 mg/L, is prepared using clear water (salinity 508 mg/L), and subsequently diluted with sewage (salinity 3700 mg/L) to yield four distinct polymer solutions with experimental concentrations of 1.4 g/L, 2.1 g/L, 3.2 g/L, and 4.5 g/L.

The experimental setup comprises a core holder measuring 2.5 cm \times 100 cm (Figure 1b), a pump operating at a consistent speed and pressure (Figure 1c), a rheometer, an incubator, a hand pump, and multiple pressure gauges. The pump utilized in the system is a high-pressure piston pump capable of pressurizing and draining liquids, conducting pressure tests, and monitoring pressure. This pump features two distinct modes: constant speed and constant pressure.

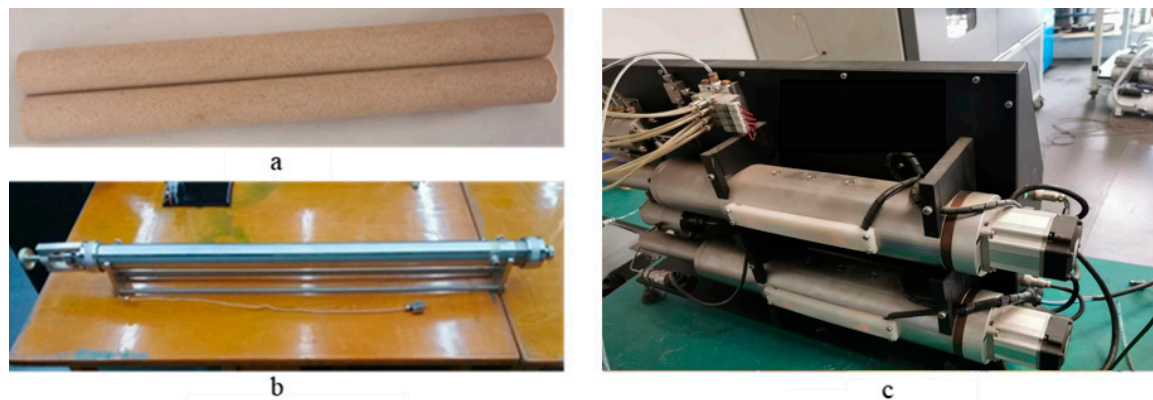


Figure 1. Apparatus for Studying the Relationship Between Viscosity and Velocity of Polymers of Different Concentrations: (a) Synthetic rock core, 300 mm in length; (b) Rock core holder, 1000 mm in length; (c) Laminar flow pump.

2.2. Experimental Scheme

To assess the viscosity loss of polymer solutions, various concentrations of solutions were injected into cores to induce shear degradation. The experiment employed a total volume of 200 mL of a salt-resistant polymer solution, with concentrations of 1.4 g/L, 2.1 g/L, 3.2 g/L, and 4.5 g/L. The shearing process took place at room temperature, subjecting four distinct salt-resistant polymer solutions to different shear rates. Subsequently, the rheometer measured the viscosity of each polymer post-shearing. (1) The core underwent a 30 min vacuumization process, followed by the saturation of pore spaces with a 3700 mg/L brine at 45 °C for a duration of 2 h. Subsequently, the stable pressure of the core was recorded under various flow conditions. To further analyze the core, the water content was calculated, and permeability measurements were conducted. (2) Seepage experiments were conducted under a flow rate of 256 mL/h, and stable pressure was recorded. (3) Following the stabilization of pressure, a core sample was meticulously extracted from the outlet for the purpose of measuring the rheological parameters of the polymer system. (4) Subsequent to the final rheological test, the injection rate was altered, and the process of repeating steps (2) and (3) was continued. At each flow rate, the viscosity of the plugging agent was tested and recorded at the core output.

2.3. Experimental Results

Figure 2 illustrates the viscosity variation curve of a salt-resistant polymer solution concerning seepage velocity. The x -axis of Figure 2 is shown in logarithmic form. The data reveal that heightened polymer concentration correlates with increased initial viscosity. Upon altering the seepage velocity from 0.0148 cm/min to 0.732 cm/min, the viscosities of the four polymers experience respective reductions of 18,330 mPa·s, 17,246 mPa·s, 7695.1 mPa·s, and 2914.1 mPa·s. The viscosity loss rates for these polymers are 87.7%, 87.6%, 81.9%, and 79.6%, sequentially. Notably, polymer solutions characterized by an elevated concentration and larger average molecular diameter exhibit a proclivity to obstruct micropores during the flow process, attributed to intermolecular entanglement, resulting in a pronounced viscosity reduction.

To integrate the rheological phenomena observed in the experiment into the numerical simulation, a power-function-fitting approach is employed to capture the relationship between viscosity and seepage velocity across various polymer conditions. The mathematical representation of the fitting curve, progressing from polymer solution A to D, is articulated as follows:

$$\mu_1 = 2634.7v_1^{-0.508} \quad (1)$$

$$\mu_2 = 2273.5v_2^{-0.507} \quad (2)$$

$$\mu_3 = 1505v_3^{-0.432} \quad (3)$$

$$\mu_4 = 798.9v_4^{-0.356} \quad (4)$$

In Figure 2, the R^2 values illustrate the level of agreement between the physical experimental data and the fitted equations for each polymer. With the R^2 scores spanning from 0.880 to 0.997, this high degree of fit confirms that the mathematical relationships from the fitting can be confidently applied to upcoming numerical simulation models.

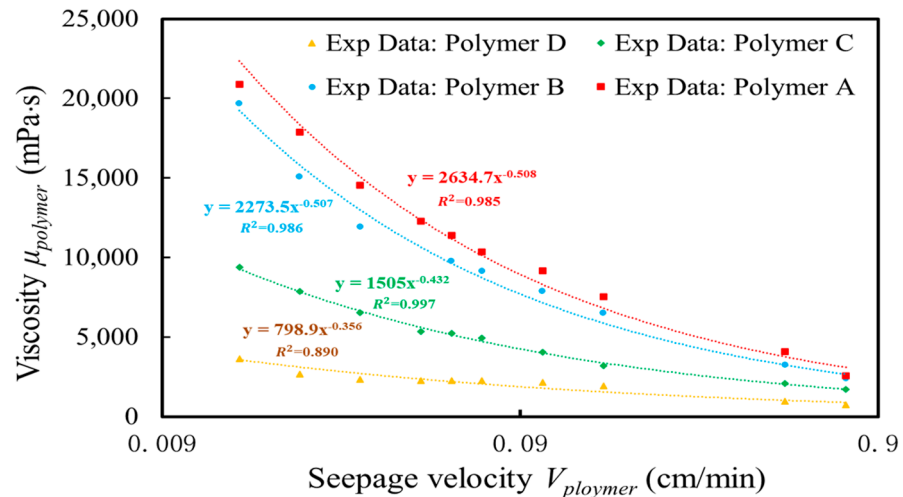


Figure 2. Correlation curves between polymer viscosity and seepage velocity.

3. Components Model Considering the Distribution of Plugging Agent

The polymer-plugging agent comprises the polymer, cross-linking agent, and gel as its primary components. Investigating the distribution patterns of the polymer-plugging agent involves considering the impact of the varying concentrations of each component on viscosity, the residual resistance coefficient, adsorption capacity, and shear-thinning characteristics. The component model is based on certain assumptions: the fluid comprises two phases (oil and water) and five components (polymer, crosslinker, gel, water, and oil); water and oil conform to Darcy's law, whereas the polymer, as a non-Newtonian fluid, adopts the flow rule obtained by the indoor experiment, that is, Formulas (1)–(4). The fluid flow is an isothermal seepage process. Additionally, Equations (1)–(4), describing the correlation between viscosity and seepage velocity, need to be integrated into the model.

The numerical simulation model encompasses the mass conservation equation, motion equation, constraint equation, and boundary conditions. The mass conservation equation, derived from the principle of mass conservation, can be uniformly expressed as follows:

$$\Delta M = M_1 - M_2 + M_3 \quad (5)$$

The constraint equations encompass the saturation constraint equation, mole fraction constraint equation, and capillary force constraint equation. The saturation constraint equation is succinctly expressed as follows:

$$S_w + S_o = 1 \quad (6)$$

where S_w and S_o are the saturations of water and oil, respectively.

The mole fraction constraint equation is represented as follows:

$$x_1 + x_2 + x_3 = 1 \quad (7)$$

$$y_1 + y_2 + y_3 = 1 \quad (8)$$

The capillary force equation is represented as follows:

$$P_w = P_o - P_{cow}(S_w) \quad (9)$$

where P_w is the pressure of the water phase, P_o is the pressure of the oil phase, P_{cow} is the capillary force of the water phase and is a function of water saturation.

Concerning inner boundary conditions, constant production rate and constant bottom hole pressure are frequently employed, and these conditions can be expressed as follows:

$$q_I = \text{const} \quad (10)$$

$$p_{wf} = \text{const} \quad (11)$$

where q_I represents the constant production rate, and P_{wf} represents the constant well flow pressure.

The initial conditions are expressed as follows:

$$P = P_i(t = 0) \quad (12)$$

$$T = T_i(t = 0) \quad (13)$$

The mass conservation equation, motion equation, constraint equation, and boundary conditions described above are discretized using different methods that are embedded in CMG. Due to the limited space of the paper, the detailed discrete forms of the mass conservation equations for water, oil, the polymer, and the crosslinking agent are not provided in the text.

4. Numerical Simulations

In this research, the CMG software (2022.10), a prevalent tool for oilfield production simulation, is employed to create 2D and 3D heterogeneous models. These models are specifically designed within the CMG framework to analyze the emplacement ratios of polymer-plugging agents in layers with different permeability levels, focusing on the variations between low-permeability and high-permeability strata. The 2D model simulates the emplacement ratio for linear displacement in fractured reservoirs (Figure 3), while the 3D model simulates the emplacement ratio for planar radial flow in reservoirs without fractures (Figure 4). Both models consist of two layers, a low-permeability layer and a high-permeability layer, with emplacement depths denoted as L_{low} and L_{high} , respectively. The study systematically analyzes the influences of the residual resistance coefficient, cumulative injection volume, average injection rate, and initial permeability ratio on the emplacement of polymer agents in different permeability layers.

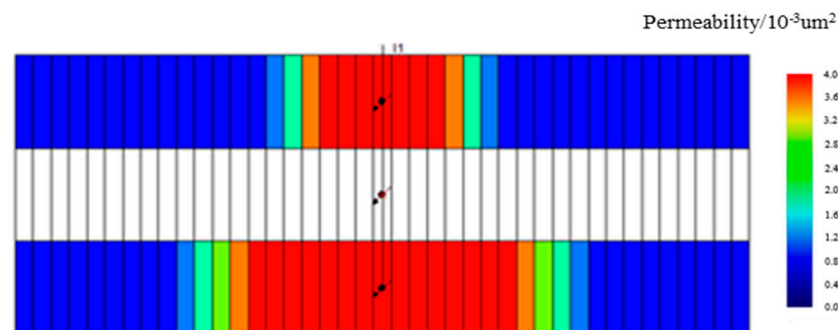


Figure 3. Two-dimensional model for modeling linear displacement.

In terms of the polymer flow characterization method, the commonly used fixed-fluid viscosity is not recommended here; instead, varying viscosity is considered according to the fitting curves obtained from the indoor experiment. To implement this process,

a customized table linking the flow rate and viscosity of the polymer is intentionally embedded in CMG.

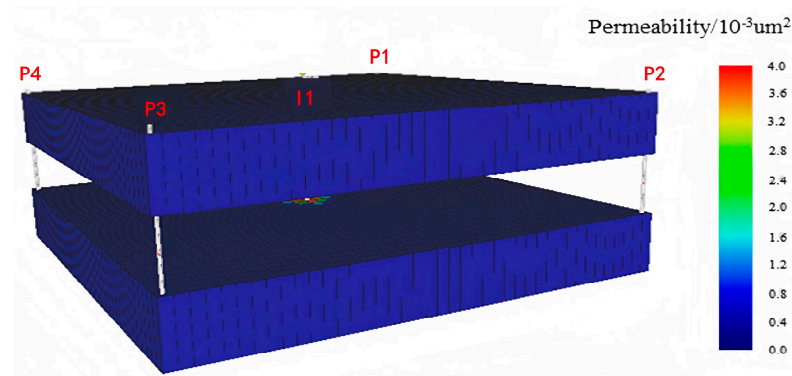


Figure 4. Three-dimensional model for modeling planar radial displacement.

4.1. The Effect of Residual Resistance Coefficient

In this section, the influence of the residual resistance coefficient on the emplacement ratios (L_{low}/L_{high}) of plugging agents with different concentrations is considered under shear-thinning and non-shear-thinning conditions. The residual resistance coefficient reflects the polymer's capability to reduce the permeability of porous media, defined as the ratio of the water-relative permeability of porous media before and after polymer flooding. The basic simulation parameters for the 2D and 3D models are detailed in Tables 1 and 2, and the results of the emplacement ratio are presented in Figures 5 and 6, respectively.

Table 1. Two-dimensional plug agent model sim params with varied residual resistance.

Parameters	Value	Unit
Cumulative injection volume	36	cm ³
Initial permeability ratio	5.65	/
Average injection rate	0.1	cm/min
Residual resistance coefficient	0.5–15	/
Number of grids	20 × 3 × 1	/
Grid size	1.48 × 1.48 × 2.1	cm
Porosity	0.27561 × 0.2986 × 0.3096	/
Permeability	223 × 620 × 1260	10 ⁻³ μm ²

Table 2. Three-dimensional plug agent model sim params with varied residual resistance.

Parameters	Value	Unit
Cumulative injection volume	1600	cm ³
Initial permeability ratio	5.65	/
Average injection rate	2	cm/min
Residual resistance coefficient	5–120	/
Number of grids	41 × 41 × 3	/
Grid size	1.48 × 1.48 × 2.1	cm
Porosity	0.27561 × 0.2986 × 0.3096	/
Permeability	223 × 620 × 1260	10 ⁻³ μm ²

As illustrated in Figure 5, in the 2D model, when the residual resistance coefficient is less than 3, the depth of plugging agent penetration into the low-permeability layer increases rapidly with the rise of the residual resistance coefficient, leading to a substantial increase in the emplacement ratio. Conversely, when the residual resistance coefficient exceeds 5, the emplacement ratio stabilizes.

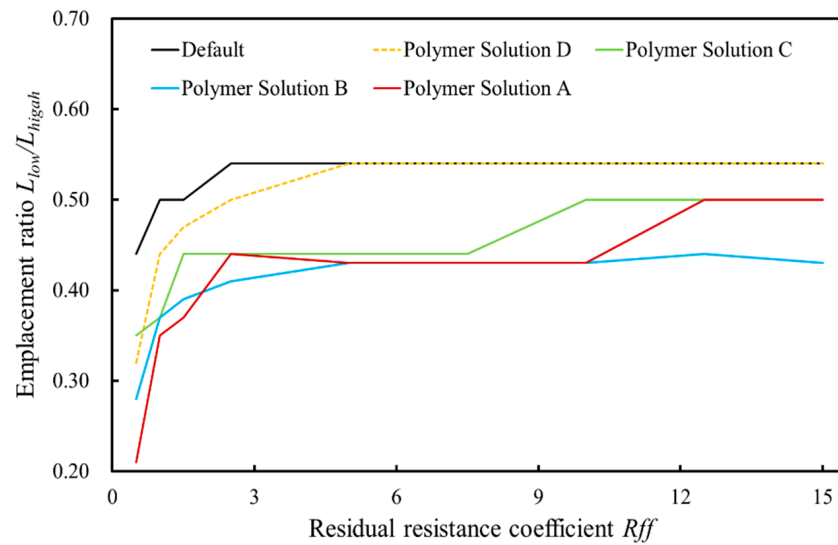


Figure 5. The effect of residual resistance on 2D plugging agent emplacement.

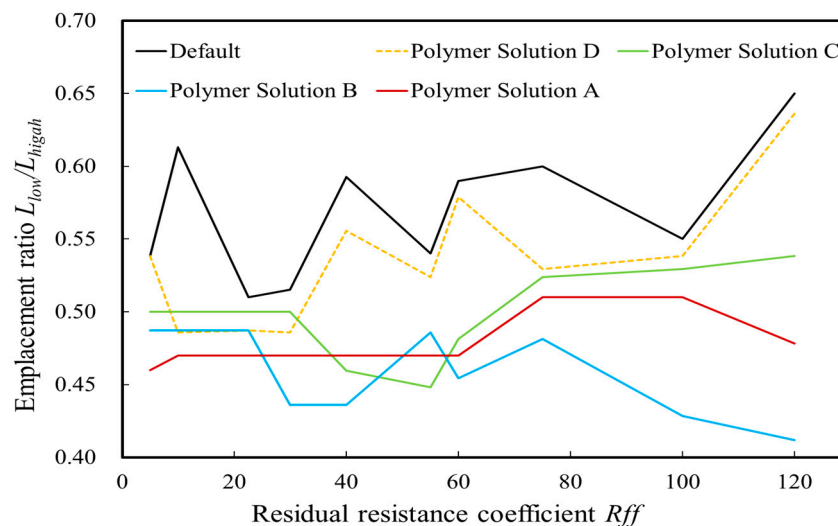


Figure 6. The effect of residual resistance on 3D plugging agent emplacement.

As depicted in Figure 6, the 3D model illustrates a dynamic fluctuation in the emplacement ratio with an increase in the residual resistance coefficient, revealing an intricate pattern. This phenomenon may be attributed to the combined effects of the emplacement depth and viscosity loss of the polymer-plugging agent. A smaller residual resistance coefficient results in a deeper penetration of the polymer-plugging agent into the low-permeability layer. With the same seepage velocity, a higher viscosity loss rate corresponds to a smaller filling ratio of the low-permeability layer to the high-permeability layer. However, under the same seepage velocity, a higher viscosity loss rate is associated with a lower emplacement ratio.

4.2. The Effect of Cumulative Injection Volume

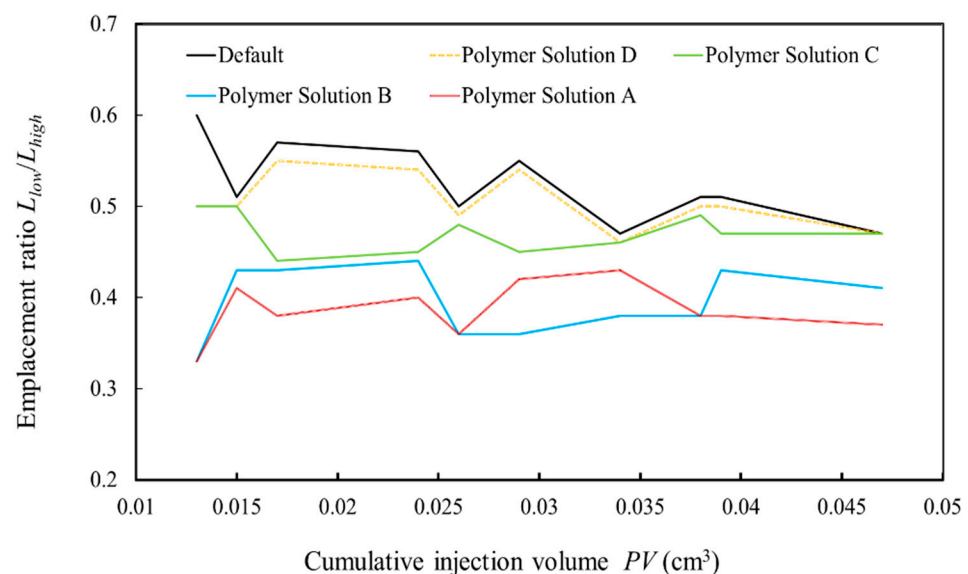
This section presents the disparity in plugging depth with and without shear thinning at various cumulative injection rates. The control of the cumulative injection volume of the polymer-plugging agent is achieved through the regulation of injection time. Parameters utilized in the 2D and 3D models are outlined in Tables 3 and 4, encompassing a diverse range of cumulative injection volumes. The emplacement ratio outcomes are shown in Figures 7 and 8.

Table 3. Two-dimensional plug agent model sim params with varying cumulative injection volume.

Parameters	Value	Unit
Cumulative injection volume	0.99–3.58	cm ³
Initial permeability ratio	5.65	/
Average injection rate	0.1	cm/min
Residual resistance coefficient	5	/
Number of grids	20 × 3 × 1	/
Grid size	1.48 × 1.48 × 2.1	cm
Porosity	0.27561 × 0.2986 × 0.3096	/
Permeability	223 × 620 × 1260	10 ⁻³ μm ²

Table 4. Three-dimensional plug agent model sim params with varying cumulative injection volume.

Parameters	Value	Unit
Cumulative injection volume	433–1534	cm ³
Initial permeability ratio	5.65	/
Average injection rate	2	cm/min
Residual resistance coefficient	5	/
Number of grids	41 × 41 × 3	/
Grid size	1.48 × 1.48 × 2.1	cm
Porosity	0.27561 × 0.2986 × 0.3096	/
Permeability	223 × 620 × 1260	10 ⁻³ μm ²

**Figure 7.** The effect of cumulative injection volume on 2D plugging agent emplacement.

Upon the introduction of the polymer-plugging agent into the reservoir, the permeability undergoes alteration, resulting in a dynamic shift in the emplacement ratio. Nevertheless, as the cumulative injection volume rises, the discrepancy in the emplacement ratio between the low permeability layer and high permeability layer progressively diminishes.

As depicted in Figures 7 and 8, the emplacement ratio of the default polymer solution consistently ranks as the highest, succeeded by polymer solutions C and D. Conversely, polymer solutions A and B exhibit the lowest emplacement ratios. Both the 2D and 3D modeling results indicate that polymer solutions A and B experience elevated viscosity loss rates, resulting in a relatively modest ratio of plugging agent emplacement depth. Consequently, at equivalent seepage velocities, a higher viscosity loss rate correlates with a diminished emplacement ratio. This, in turn, leads to a reduced amount of plugging agent infiltrating the low permeability layer, thereby enhancing the plugging efficacy in the high permeability layer.

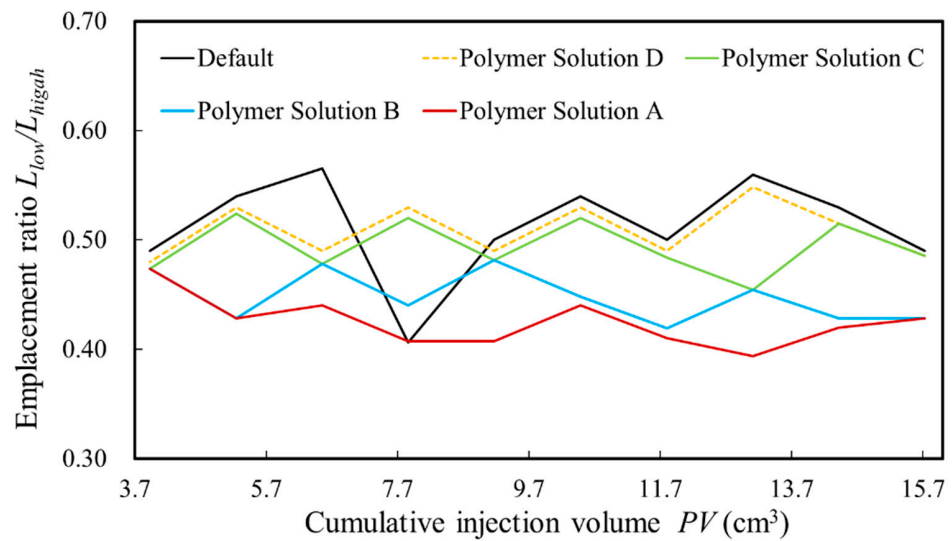


Figure 8. The effect of cumulative injection volume on 3D plugging agent emplacement.

4.3. The Effect of Average Injection Rate

The examination of the impact of the average injection rate on the emplacement ratio of the plugging agent is conducted under both shear-thinning and non-shear-thinning conditions. Simulation parameters are detailed in Tables 5 and 6, with the respective results graphically presented in Figures 9 and 10.

Table 5. Two-dimensional plug agent model sim params with varying average injection rate.

Parameters	Value	Unit
Cumulative injection volume	36	cm ³
Initial permeability ratio	5.65	/
Average injection rate	0.01–0.6	cm/min
Residual resistance coefficient	5	/
Number of grids	20 × 3 × 1	/
Grid size	1.48 × 1.48 × 2.1	cm
Porosity	0.27561 × 0.2986 × 0.3096	/
Permeability	223 × 620 × 1260	10 ^{−3} μm ²

Table 6. Three-dimensional plug agent model sim params with varying average injection rate average.

Parameters	Value	Unit
Cumulative injection volume	1600	cm ³
Initial permeability ratio	5.65	/
Average injection rate	0.008–0.44	cm/min
Residual resistance coefficient	5	/
Number of grids	41 × 41 × 3	/
Grid size	1.48 × 1.48 × 2.1	cm
Porosity	0.27561 × 0.2986 × 0.3096	/
Permeability	223 × 620 × 1260	10 ^{−3} μm ²

As illustrated in Figure 9, within the 2D model and constrained by an injection rate of 0.1 cm/min, the emplacement ratio undergoes a distinct variation. For injection rates below 0.1 cm/min, an incremental injection rate leads to dynamic changes in the depth of plugging agent penetration into the reservoir. Conversely, stability is observed after the injection rate surpasses 0.1 cm/min. Figure 10 reveals that, in the 3D model, the emplacement ratio experiences a rapid increase with the injection rate until it reaches 0.1 cm/min, after which the ratio remains relatively constant. A higher viscosity loss rate at the same seepage velocity leads to a lower emplacement ratio.

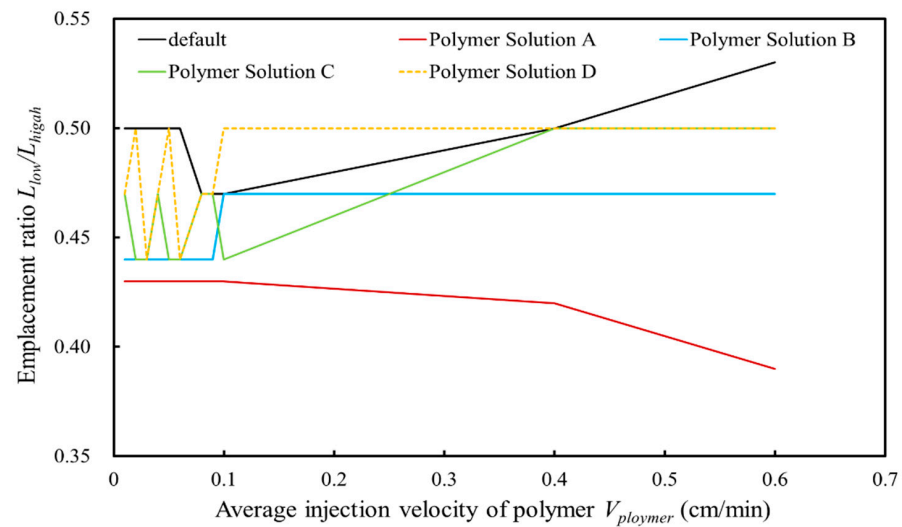


Figure 9. The effect of average injection rate on 2D plugging agent emplacement.

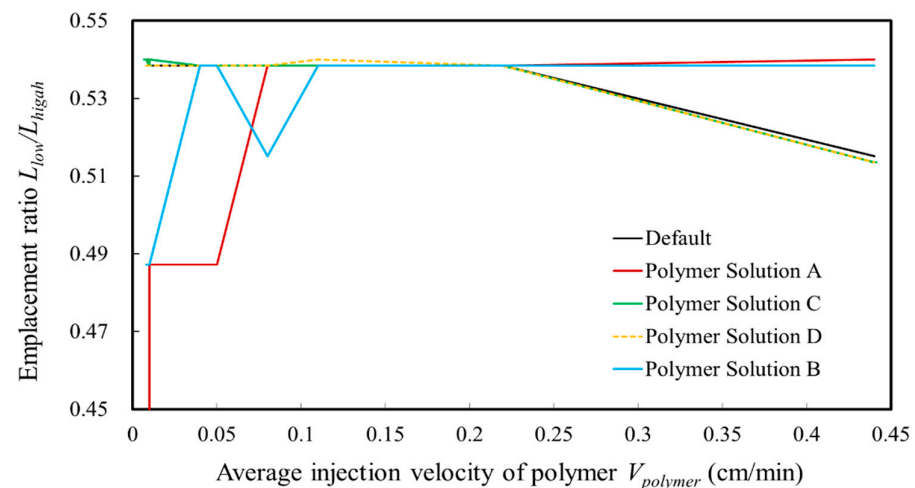


Figure 10. The effect of average injection rate on 3D plugging agent emplacement.

4.4. The Effect of Initial Permeability Ratio

Permeability differentiation, being a significant manifestation of reservoir heterogeneity, holds a pivotal influence on the emplacement depth of water-plugging agents. To quantify the differentiation degree of initial permeability distribution, the initial permeability ratio is introduced. Simulation parameters, encompassing a diverse permeability ratio ranging from 5.82 to 34.7, are summarized in Tables 7 and 8.

Table 7. Two-dimensional plug agent model sim params with varying average initial permeability ratio.

Parameters	Value	Unit
Cumulative injection volume	36	cm ³
Initial permeability ratio	5.82–34.7	/
Average injection rate	0.1	cm/min
Residual resistance coefficient	5	/
Number of grids	20 × 3 × 1	/
Grid size	1.48 × 1.48 × 2.1	cm
Porosity	0.27561 × 0.2986 × 0.3096	/
Permeability	223 × 620 × 1260	10 ^{−3} μm ²

As depicted in Figures 11 and 12, the emplacement ratio consistently positions the default polymer solution as the highest, with polymer solution A exhibiting the lowest

emplacement ratio. In both the 2D and 3D models, an increase in the initial permeability ratio corresponds to a decrease in the emplacement ratio, along with a reduction in the fraction of the plugging agent penetrating the low permeability layer. In reservoirs characterized by highly differentiated permeability, plugging agents exhibit enhanced effectiveness, minimizing polymer wastage in low permeability layers. Furthermore, at equivalent seepage velocities, a higher viscosity loss rate for the polymer-plugging agent results in a smaller emplacement ratio, achieving the same plugging endpoint.

Table 8. Three-dimensional plug agent model sim params with varying average initial permeability ratio.

Parameters	Value	Unit
Cumulative injection volume	1600	cm ³
Initial permeability ratio	5.82–34.7	/
Average injection rate	2	cm/min
Residual resistance coefficient	5	/
Number of grids	41 × 41 × 3	/
Grid size	1.48 × 1.48 × 2.1	cm
Porosity	0.27561 × 0.2986 × 0.3096	/
Permeability	223 × 620 × 1260	10 ⁻³ μm ²

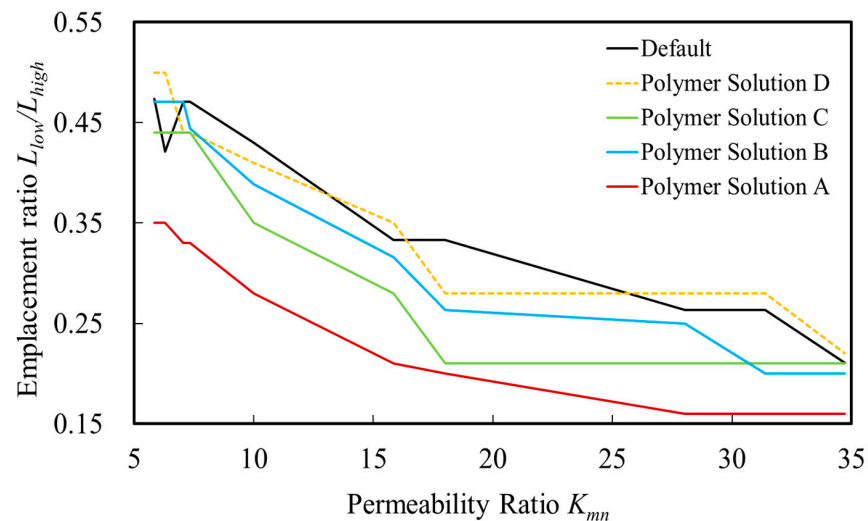


Figure 11. The effect of permeability difference on 2D plugging agent emplacement.

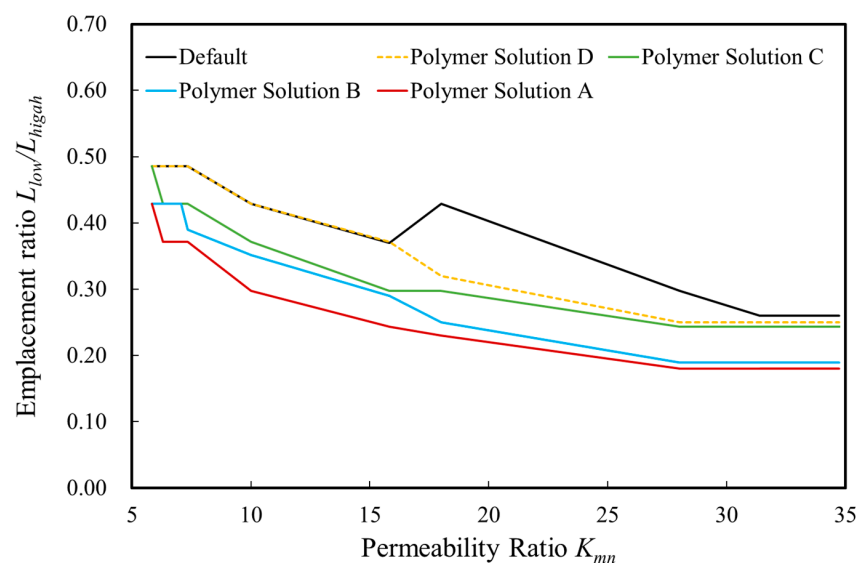


Figure 12. The effect of permeability difference on 3D plugging agent emplacement.

4.5. Multivariate Regression Analysis

The numerical simulation results elucidate the impact of the residual resistance coefficient, cumulative injection volume, initial permeability ratio, and average injection rate on the emplacement ratio of the polymer-plugging agent. Utilizing regression analysis with these key parameters, the emplacement ratio can be predicted, offering valuable insights for water-plugging agent selection in heterogeneous reservoirs. In Equations (14)–(23), where y denotes the plugging agent emplacement ratio, x_a , x_b , x_c , and x_d represent the residual resistance coefficient, cumulative injection volume, initial permeability ratio, and average injection rate, respectively. Each set of fitting equations comprises four different polymer solution concentrations and one default group. The comparison between numerical-simulation results and nonlinear-regression-fitting results is illustrated in Figures 13 and 14, demonstrating satisfactory fitting performance achieved through multivariate nonlinear regression.

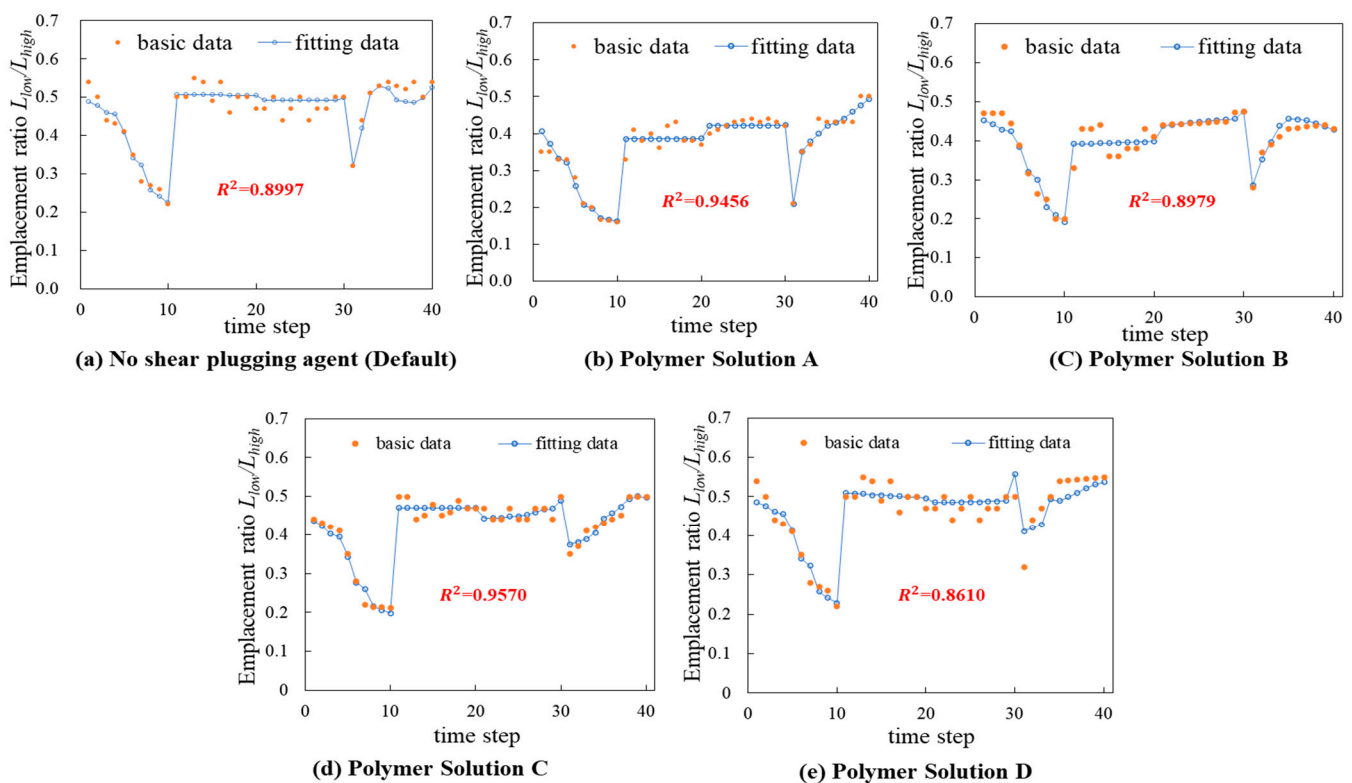


Figure 13. Multivariate nonlinear regression of 2D model.

(1) Multivariate nonlinear regression of 2D model

We employed the CMG software to assess the impact of various plugging agents on oilfield productivity. Relying on CFD principles and integrating key parameters such as residual resistance coefficients and injection volumes, the software predicts the effectiveness of the plugging agents. The numerical simulation data (basic data) from CMG, analyzed through multivariate nonlinear regression, resulted in “fitting data” curves. This aims to establish a precise mathematical relationship between the plugging agent’s emplacement ratio and essential influencing factors. As illustrated in Figures 13 and 14, the meticulous fitting of the 2D and 3D model data has yielded equations that provide a quantitative basis for reservoir management, aiding in enhancing production capacity.

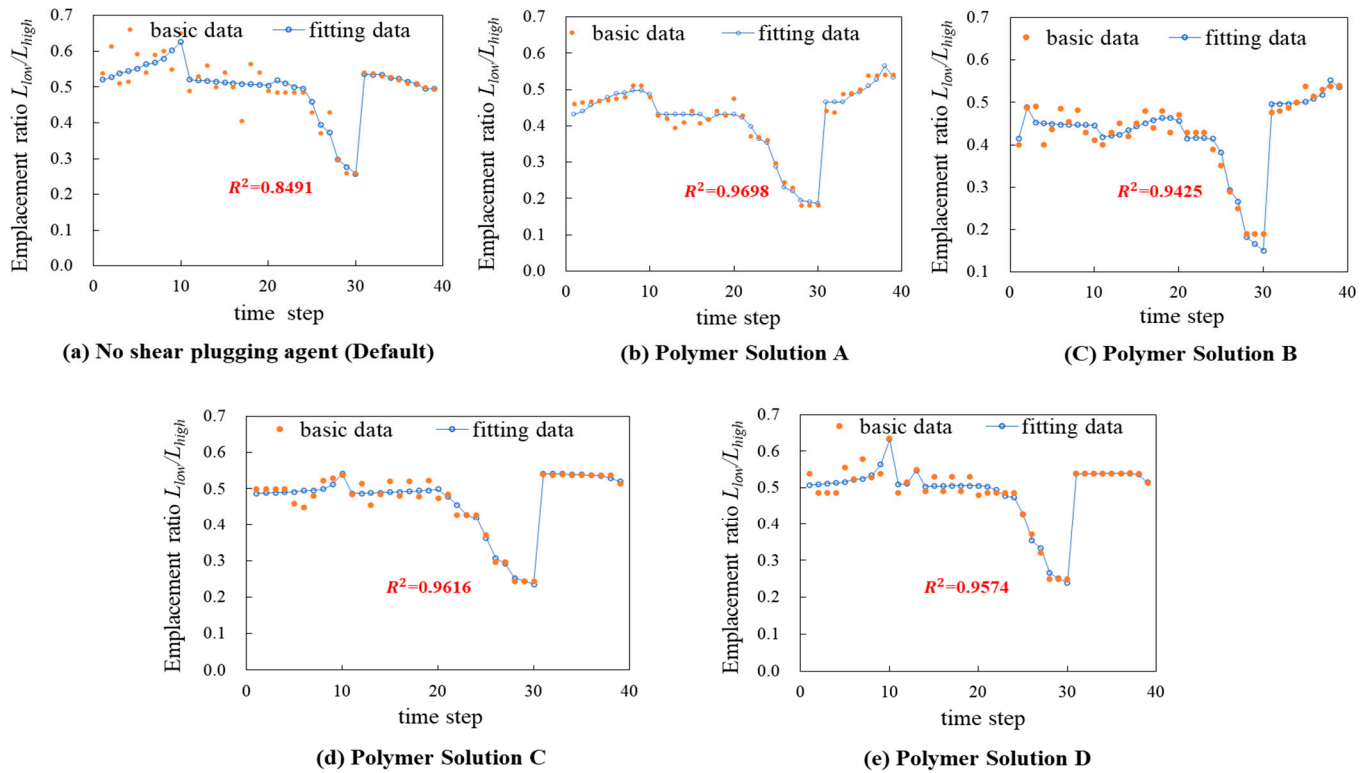


Figure 14. Multiple nonlinear regression of 3D model.

Figure 13's R^2 values indicate high accuracy in the fitting results. R^2 values range from 0 to 1, where values closer to 1 signify a better match between the fitted and original data. The 'Default (No shear)' has a strong correlation at 0.8997. 'Polymer Solution A' is an excellent fit at 0.9456, while 'Polymer Solution B' is also robust at 0.8979. 'Polymer Solution C' leads with an R^2 of 0.9570, showing a tight match with the data. 'Polymer Solution D', although the lowest, is still a solid fit at 0.8610. These high R^2 values suggest that the model provides a precise fit across all solutions.

(2) Regression equation of 2D model

$$y = [179.3 - 89.63 \times \ln x_a - 0.622 \times (\ln x_b)^2 - 168.14 \times \ln x_c - 72.23 \times (\ln x_d)^2 + 19.99 \times (\ln x_d)^3] \div (1 - 342.02 \times \ln x_3 - 112.51 \times \ln x_4) \quad (14)$$

$$y = [1.18 + 0.1 \times \ln x_a - 0.11 \times (\ln x_b)^2 + 1.46 \times x_c + 0.015 \times x_d^2 + 0.00029 \times x_d^3] \div (1 + 1.55 \times \ln x_a - 0.31 \times (\ln x_b)^2 + 3.39 \times x_c + 0.04 \times x_d^2) \quad (15)$$

$$y = [1.448 - 1.61 \times \ln x_a - 0.027 \times (\ln x_b)^2 + 18.13 \times x_c + 0.18 \times x_d^2 - 0.0014 \times x_d^3] \div [1 - 0.99 \times \ln x_a - 0.193 \times (\ln x_b)^2 + 36.8 \times x_c + 0.37 \times x_d^2] \quad (16)$$

$$y = (3.17 + 0.28 \times x_a + 0.004 \times x_b^2 - 0.006 \times x_c + 0.019 \times x_d^2) \div (1 + 2.48 \times x_a + 0.01 \times x_b^2 - 0.05 \times x_c^3 - 1.2 \times x_d + 0.086 \times x_d^2) \quad (17)$$

$$y = (1.9 + 0.017 \times x_a - 0.07 \times x_b + 3.83 \times x_c^2 + 0.037 \times x_d^3) \div (1 + 0.4 \times x_a - 0.0035 \times x_b^2 + 0.013 \times x_c + 0.06 \times x_d^2 + 0.065 \times x_d^3) \quad (18)$$

(3) Multiple nonlinear regression of 3D model

Figure 14 shows the data and fitting curves for different blockers in a 3D simulation model, with high R^2 values indicating accurate results. 'Default (No shear)' is strongly correlated at 0.8491, 'Polymer Solution A' fits excellently at 0.9698, 'Polymer Solution B' is robust at 0.9425, 'Polymer Solution C' is outstanding with an R^2 of 0.9616, and 'Polymer

Solution D', though the lowest, still fits well at 0.9574. These values demonstrate the model's precise fit for all solutions.

(4) 3D model regression equation

$$y = \left[\frac{0.5076 - 0.0167 \times \ln x_a - 0.008 \times (\ln x_b)^2 - 0.0006 \times x_c + 0.037 \times x_d^2 - 0.0135 \times x_d^3}{1 - 0.033949 \times \ln x_a - 0.01643 \ln x_b^2 + 0.0018 \times \ln x_c^3 + 0.039 \times x_d^4} \right] \quad (19)$$

$$y = \left[\frac{-6.249 + 0.037x_a - 0.0002x_a^2 + 0.219x_c^2 + 1.01x_d^3}{1 - 7.73x_a^3 + 1.4x_c^2 - 3.04x_d + 6.26x_d^2} \right] \quad (20)$$

$$y = \left(\frac{0.306 - 0.365 \times \ln x_a + 0.0026 \ln x_b^2 + 0.024x_c + 0.003x_d^2 + 0.0167x_d^3}{1 - 0.825 \ln x_a + 0.000116x_b + 0.0045x_c^2 + 0.044x_d^3} \right) \quad (21)$$

$$y = \left(\frac{0.523 - 0.0071 \ln x_a - 0.0089 \ln x_b^2 + 0.0014 \ln x_c^3 - 0.003x_d}{1 - 0.0148 \ln x_a - 0.0179 \ln x_b^2 + 0.01x_c - 0.001x_d^2} \right) \quad (22)$$

$$y = \left(\frac{0.7 - 0.0018x_a + 0.0000006x_b^2 + 0.0000004x_c^3 + 0.058x_d - 0.49x_d^2}{1 - 0.0038x_a + 0.00000011x_b^2 + 0.023x_c + 0.5x_d^2 - 0.679x_d^3} \right) \quad (23)$$

5. Application

Due to the considerable heterogeneity inherent in most oil and gas reservoirs, the precise calculation of plugging agent quantities and the prediction of their distribution pose challenges without real-time monitoring. On-site water plugging and profile control encounters a significant obstacle when the plugging agent migrates from the substantial channels within high permeability layers to the designated profile control radius, while those within lower permeability layers may not have reached the corresponding locations. In this context, the regression mathematical model proposed in this study offers an accurate means of calculating plugging agent dosage. The total amount of plugging agent can be determined by understanding the depth of the plugging agent in various permeability layers.

This mathematical model has been successfully applied to the Kunan Oilfield block, as illustrated in Figures 15 and 16. According to the provided statistics, the geological reserves within the block amount to 394,300 tons, with a cumulative oil production from the well group reaching 103,000 tons, resulting in a recovery rate of 25.06%. The permeabilities of the three primary oil-bearing layers are as follows: $900 \times 10^{-3} \mu\text{m}^2$, $632 \times 10^{-3} \mu\text{m}^2$, $300 \times 10^{-3} \mu\text{m}^2$, and $140 \times 10^{-3} \mu\text{m}^2$, with the mean value of $493 \times 10^{-3} \mu\text{m}^2$.

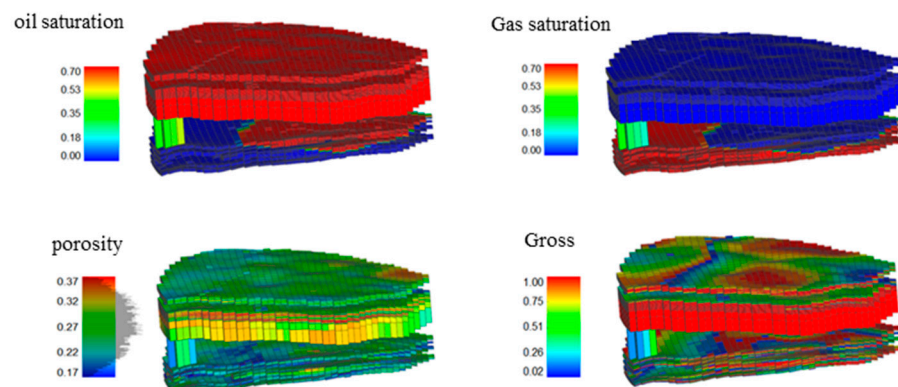


Figure 15. Schematic diagram showing oil and gas content and saturation in Kunan Oilfield.

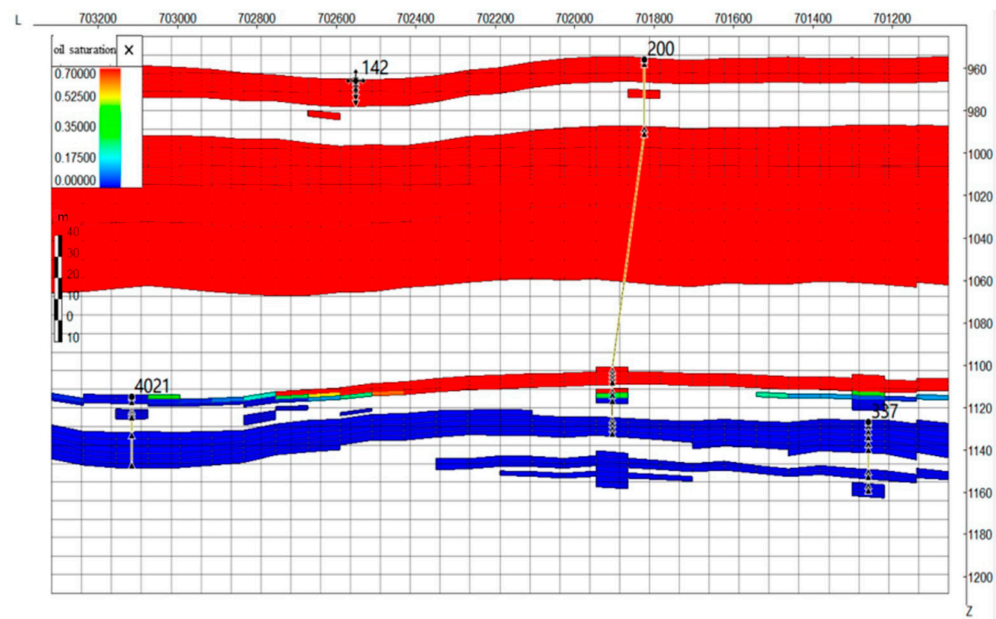


Figure 16. Vertical profile of oil saturation in Kunan Oilfield.

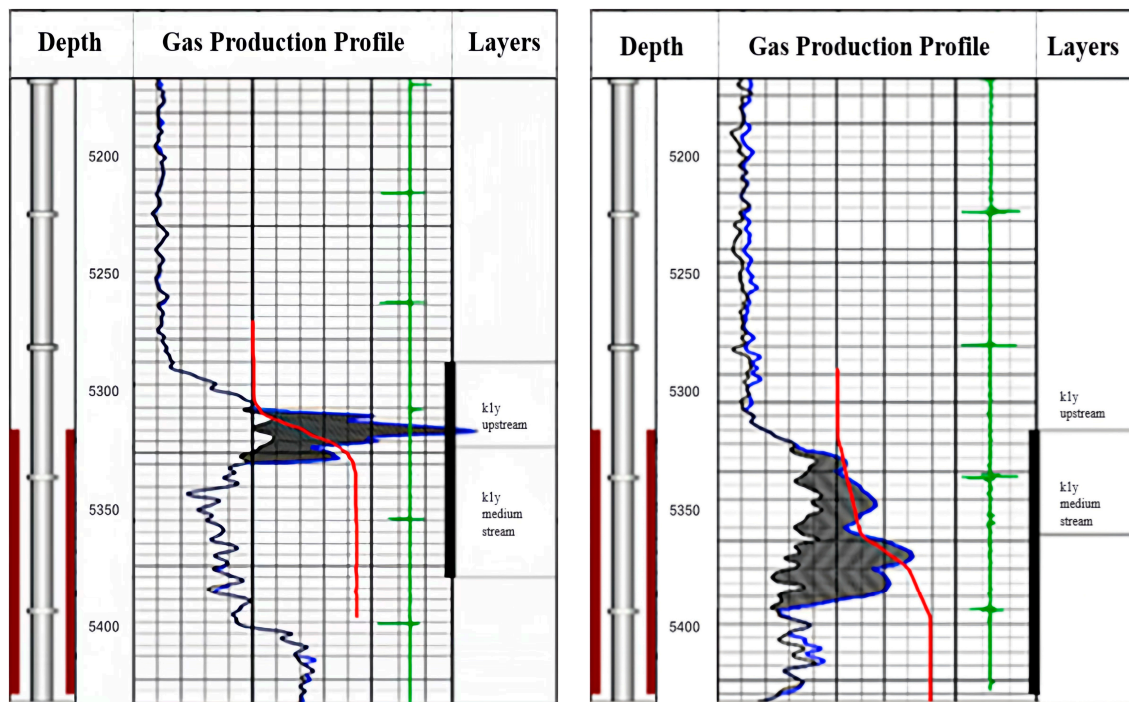
A salt-resistant polymer solution, with a concentration of 1.4 g/L, was employed in the Kunan Oilfield block. Utilizing a regression mathematical model (residual resistance coefficient $x_a = 1.5$, cumulative injection rate $x_b = 5000$, initial permeability ratio $x_c = 6.4$, average injection rate $x_d = 500$), the emplacement ratio of the plugging agent γ is determined to be 4. Accounting for a profile control radius equal to 1/3 of the well spacing in the high permeability layer, the profile control distance for the high permeability layer is set at 100 m. The profile control radii for the other two low-permeability layers are determined to be 25 m and 6.25 m, respectively. This result obtained from the model simulation and the water profile obtained from the field-measured logging data can be well matched and fitted. Table 9 presents the specific setup parameters for the Kunan Oilfield block.

Table 9. Parameters of three horizons in the block of Kunan Oilfield.

Parameters	Value	Unit
Effective porosity	0.27	/
oil saturation	0.49	/
Surface crude oil density	821	kg/m ³
Volume factor	1.1	/
Profile control radius (1)	100	m
Profile control radius (2)	25	m
Profile control radius (3)	6.25	m
Effective thickness	101	m
The difference of penetration depth of plugging agent in different permeability layers is not considered	3.84×10^6	m ³
Wang Juan's calculation method [16]	2.16×10^6	m ³
Considering the difference of penetration depth of plugging agent in different permeability layers	6.25	m ³

The calculated amount of plugging agent, derived from the mathematical model, serves as a guide for profile control. Post-implementation, there is a notable enhancement in the water absorption profile, increasing the thickness of the water absorption layer from 5 m (Figure 17a) to 12 m (Figure 17b). The preliminary validation of the mathematical model is evident through field records. The further refinement of the regression model is essential to enhance its adaptability, and future efforts may explore the utilization of fuzzy mathematics to assign weights to key parameters. Simultaneously, clarifying the

correlation between control parameters is imperative. Due to space constraints, a thorough discussion on these aspects is not possible here. Nevertheless, the research in this study holds reference significance for the efficient development of heterogeneous reservoirs.



(a) (14 April 2019)

(b) (21 November 2020)

Figure 17. Water injection profile before profile control.

6. Conclusions

In this study, an artificial core experiment device is configured to assess the plugging efficiency of a polymer-plugging agent under varying seepage velocities, with the findings subsequently integrated into two- and three-dimensional heterogeneous models through component-numerical simulation, which is validated in an application study. The following findings can be drawn:

- (1) The relationship between the flow velocity and viscosity of four types of plugging agents was tested using artificial core experimental methods, and corresponding equations were established for numerical simulation research;
- (2) Two-dimensional and three-dimensional heterogeneous models were established through numerical simulation; the ratio of the residual resistance coefficient, cumulative injection volume, permeability gradient, and average injection rate to the depth of polymer-plugging agents entering low-permeability layers and high-permeability layers was studied; by comparing the entry depth of plugging agents under shear-thinning conditions and non-shear thinning conditions, it was found that under the same flow rate conditions, the higher the viscosity loss rate, the smaller the ratio;
- (3) Based on the numerical simulation results of the different types of plugging agents, multiple nonlinear regression methods were used to establish corresponding mathematical models; the R-squared value of the fitting degree between the two was between 0.85 and 0.96, indicating accurate fitting;
- (4) The mathematical model results fitted in this study were applied to a certain block in the Kunan Oilfield; after profile control, the thickness of the water-absorbing layer changed from the original 5 m to the current 12 m; the actual construction results show that the mathematical model calculation results in this article are reliable.

The proposed model and established regression model are conducive to the understanding of the plugging agent distribution and dosage estimation, which lays a good theoretical foundation for the effective and efficient reservoir exploitation of crude oil. The research in this paper has guiding significance for the secondary development of oil reservoirs with different permeability layers. The research work in this paper is a preliminary exploration of the properties and performance of water-plugging agents in reservoir development, and a larger-scale field application and comparison with field results is needed, which will be a promising direction for future research.

Author Contributions: Conceptualization, S.H.; Methodology, S.H. and C.X.; Software, C.X.; Validation, C.D.; Formal analysis, C.D.; Investigation, Y.M.; Resources, Y.M.; Data curation, S.L.; Writing—Original draft, S.H.; Writing—Review & editing, S.L., L.G. and S.W.; Visualization, J.Z.; Supervision, J.Z., L.G. and S.W. All authors have read and agreed to the published version of the manuscript.

Funding: This research was funded by the National Natural Science Foundation of China, under the project ‘Study and Application of Permeation Mechanics in Enhanced Oil Recovery in High Permeability and High Water-Cut Thin Oil Reservoirs’ (Grant No. 52374051).

Data Availability Statement: Data are contained within the article.

Conflicts of Interest: Author Shanbin He, Chunqi Xue, Chang Du, Yahui Mao, Shengnan Li were employed by Changqing Oilfield Company. The remaining authors declare that the research was conducted in the absence of any commercial or financial relationships that could be construed as a potential conflict of interest.

Nomenclature

F	Discrete equation of four components
K_{ro}	Relative permeability of oil phase
K_{rg}	Relative permeability of gas phase
K_{rw}	Relative permeability of water phase
L_{low}	Depth of polymer solution entering low permeability
L_{high}	Depth of polymer solution entering high permeability
P_o	The pressure of oil phase
P_w	The pressure of water phase
P_g	The pressure of gas phase
X_a	Residual resistance coefficient
X_b	Cumulative injection volume
X_c	Initial permeability ratio
X_d	Average injection rate
X	Variable to be solved
T	Reservoir temperature
μ	Viscosity
v	Seepage velocity
y	Emplacement ratio
ΔM	The change in the amount of substance
M_1	The initial amount
M_2	The amount that has left the system
M_3	The amount that has entered or been generated within the system
S_{wr}	Residual water saturation
S_o	Oil saturation
$V_{i\pm 1/2,j,k}^{n+1}$	The flow velocity at the node $i \pm 1/2, j, k$ at time step $n + 1$
k_x	The absolute permeability in the x direction
$k_{r,i\pm 1/2,j,k}^{n+1}$	The relative permeability at the node $i \pm 1/2, j, k$ at the time step $n + 1$
$P_{i,j,k}^{n+1}$	The pressures at nodes i, j, k and $i + 1, j, k$ respectively, at time step $n + 1$
μ	The viscosity of the fluid

Δx	The size of the grid cell in the x direction
Δy	The size of the grid cell in the y direction
Δz	The size of the grid cell in the z direction
Δt	Time step
ϕ	Porosity of the rock
ρ	Fluid density
V	Components of the velocity vector, with subscripts x, y, z indicating components in the x, y, z directions, respectively
$F_m(X + \delta X)$	The value of the function F_m near the point X
$F_m(X)$	The value of the function F_m at point X
Σ	The summation symbol
δx_i	The small increment in the variable X_i
$o(\delta X^2)$	Represents higher-order infinitesimals
$\frac{\partial F_m}{\partial x_i}$	The partial derivative of the function F_m concerning the variable x_i

References

- Cao, B.; Xie, K.; Lu, X.; Cao, W.; He, X.; Xiao, Z.; Zhang, Y.; Wang, X.; Su, C. Effect and mechanism of combined operation of profile modification and water shutoff with in-depth displacement in high-heterogeneity oil reservoirs. *Colloids Surf. A Physicochem. Eng. Asp.* **2021**, *631*, 127673. [\[CrossRef\]](#)
- Wang, S.; Yu, C.; Sang, G.; Yu, R.; Cheng, F. An oil–water two-phase reservoir numerical simulation coupled with dynamic capillary force based on the full-implicit method. *Comput. Math. Appl.* **2020**, *79*, 2527–2549. [\[CrossRef\]](#)
- Xiong, C.; Tang, X. Technologies of water shut-off and profile control: An overview. *Pet. Explor. Dev.* **2007**, *1*, 83–88.
- Chen, T. Research on Influence Factors and Regulatory Methods of Sweep Coefficient and Displacement Efficiency of SP Combination Flooding for Heavy Oil. Ph.D. Thesis, China University of Petroleum (East China), Qingdao, China, 2014.
- Gao, S. *Polymer Flooding Improves Oil Recovery*; Petroleum Industry Press: Beijing, China, 1996.
- Sun, Z.; Wu, X.; Kang, X.; Lu, X.; Li, Q.; Jiang, W.; Zhang, J. Comparison of oil displacement mechanisms and performances between continuous and dispersed phase flooding agents. *Pet. Explor. Dev.* **2019**, *46*, 121–129. [\[CrossRef\]](#)
- Liu, W.; Lin, C.; Yang, Y. A new method for quantitatively identifying advanced channeling paths in thick reservoirs with low permeability. *J. Oil Gas Technol.* **2010**, *32*, 1–5.
- Zhao, X.; Wang, C. A Study on Microscopic Profiling/Oil Displacing Mechanisms in Weak Gel Flooding. *Oilfield Chem.* **2004**, *21*, 56–60.
- Bin Marta, E.S.; Hammouda, M.M.M.S.; Tantawy, M.A.; Khamis, M.A.; Wahba, A.M. Diagnosing and Controlling Excessive Water Production: State-of-the-Art Review. *J. Pet. Min. Eng.* **2023**, *25*, 9–25. [\[CrossRef\]](#)
- Tang, Y. Research on the Determination Methods of Blocking Agent Injection Depth or Position. Master's Thesis, China University of Petroleum (East China), Qingdao, China, 2014.
- Li, Y.; Tan, H.; Cai, L. Current Situation and Development Direction of Water Shutoff & Profile Control in China. *Drill. Prod. Technol.* **2006**, *29*, 105–106.
- Scott, T.; Roberts, L.J.; Sharpe, S.R.; Clifford, P.J.; Sorbie, K.S. In-Situ Gel Calculations in Complex Reservoir Systems Using a New Chemical Flood Simulator. *SPE Reserv. Eng.* **1987**, *2*, 634–646. [\[CrossRef\]](#)
- Deppe, J.C. Injection rates- the effect of mobility ratio, area swept, and pattern. *Soc. Pet. Eng. J.* **1961**, *1*, 81–91. [\[CrossRef\]](#)
- Lano, J.T.; Lee, R.L.; Seright, R.S. Gel Placement in Production Wells. *Met. Powder Rep.* **2011**, *19*, 156–164.
- Seright, R.S. Placement of Gels to Modify Injection Profiles. *Enhanc. Oil Recovery Symp.* **1988**, *32*, 137–148.
- Ates, H.; Kasap, E.; Tomutsa, L.; Gao, H.W. Use of statistical dispersion model to study polymer clogging in sandstone samples. In Proceedings of the SPE/DOE Improved Oil Recovery Symposium, Tulsa, OK, USA, 21–24 April 2010.
- Foster, W.R. A low-tension water flooding process. *J. Pet. Technol.* **1973**, *25*, 205–210. [\[CrossRef\]](#)
- Wang, J.; Wang, S.; Lin, W.; Kang, Z. Identification and control of vertical distribution of polymer gel plugging agent. *Fault-Block Oil Gas Field* **2018**, *25*, 93–96.
- Jin, B.; Jiang, H.; Zhang, X.; Wang, J.; Yang, J.; Zheng, W. Numerical simulation of surfactant polymer flooding. *Chem. Technol. Fuels Oils* **2014**, *50*, 55–70. [\[CrossRef\]](#)
- Smith, J.E. The transition pressure: A quick method for quantifying polyacrylamide gel strength. In Proceedings of the SPE International Symposium on Oilfield Chemistry, Houston, TX, USA, 8–10 February 1989; Volume 1, pp. 473–480.
- Daripa, P.; Mishra, R. Modeling shear thinning polymer flooding using a dynamic viscosity model. *Phys. Fluids* **2023**, *35*, 046606. [\[CrossRef\]](#)
- Zhang, B. Effect of shear and SRB on viscosity of polymer solution prepared by sewage. *Inn. Mong. Petrochem. Ind.* **2013**, *39*, 28–29.
- Chen, W.; Wang, X.; Hu, K.; Zhuyue, W.; Zhang, J.; Wang, H. Synthesis and Properties of Polyacrylamide Polymer Flooding Agent with High Shear Resistance. *J. Xi'an Shiyou Univ. (Nat. Sci. Ed.)* **2018**, *33*, 105–111.
- Zhao, W.; Chen, S.; Jiao, Q. Performance Properties of Polymer Solutions and Gels under Shearing in Various Modes. *Oilfield Chem.* **2008**, *3*, 256–260.

-
25. Zhang, S. Study on critical concentration of dynamic gelation of new chromium crosslinker. *Chem. Eng.* **2019**, *33*, 75–77.
 26. Xu, X.; Wang, Y.; He, H.; Li, D.; Qi, Z. Research Advances in Influencing Factors of Dynamic Gelling Process of Cross-linked Polymer System in Porous Media. *Oilfield Chem.* **2014**, *31*, 312–316.

Disclaimer/Publisher's Note: The statements, opinions and data contained in all publications are solely those of the individual author(s) and contributor(s) and not of MDPI and/or the editor(s). MDPI and/or the editor(s) disclaim responsibility for any injury to people or property resulting from any ideas, methods, instructions or products referred to in the content.